Available online at www.sciencedirect.com
SCIENCE DIRECT®
Journal of Sound and Vibration 286 (2005) 763–780
JOURNAL OF SOUND AND VIBRATION
www.elsevier.com/locate/jsvi

A higher order finite element theory for buckling and vibration analysis of initially stressed composite sandwich plates

A.K. Nayak, S.S.J. Moy, R.A. Shenoi*

Ship Science, School of Engineering Sciences, University of Southampton, Highfield, Southampton SO17 1BJ, UK

Received 13 November 2003; received in revised form 11 October 2004; accepted 18 October 2004
Available online 25 February 2005

Abstract

A simple isoparametric assumed strain finite element formulation incorporating a third-order polynomial displacement model for the buckling and vibration analysis of initially stressed composite sandwich laminates is presented. The displacement model involves a nonlinear distribution of in-plane displacements through the plate thickness; the theory does not require shear correction coefficients. A nine-noded quadratic Lagrangian two-dimensional element is used with three displacements, two rotations of the normals about the plate midplane, and two warps of the normals. Full integration is carried out to evaluate various terms in the energy formulation. A consistent mass matrix is employed to preserve the total kinetic energy of the system. The accuracy of the present formulation is verified with the existing results in the literature. Numerical results are presented for the stability and free vibration of initially stressed composite sandwich plates.

1. Introduction

Composite sandwich plates are utilized in many weight-sensitive applications, where they have many advantages relative to traditional isotropic materials. However, during their build and fabrication, sandwich structures are subjected to various inplane loads which can lead to rapid failure. Hence the effects of initial stresses on the stability and vibration response of composite sandwich plates have become an active field of research in recent years.

*Corresponding author. Tel.: +44 (0) 23 80 592356; fax: +44 (0) 23 80 593299.
E-mail address: r.a.shenoi@ship.soton.ac.uk (R.A. Shenoi).

0022-460X/$ - see front matter © 2004 Elsevier Ltd. All rights reserved.
doi:10.1016/j.jsv.2004.10.055

To simulate such above-mentioned critical situations adequately, three-dimensional analysis methods [1–10] are used to get the exact results, usually at very high computational costs. Two-dimensional models, however, are preferred in practical situations: in these the number of displacement variables is kept constant and independent of the number of constitutive layers. It is quite well known that the classical laminate plate theory (CLPT) based on the Kirchhoff–Love hypothesis is inadequate for thicker plates and gives satisfactory results only for thin laminates [9]. Hence, a variety of refined shear deformable plate theories are proposed to model both thin and thick plates in a single formulation. The first-order shear deformation theory (FSDT) on Mindlin–Reissner assumptions requires the use of either constant (FSDTC) [11] or variable (FSDTV) shear correction factors. These can be calculated from shear strain energy [12], complementary shear energy [13] and predictor–corrector methods [6]. To circumvent the above difficulties, several approaches to extend FSDT either to the higher-order shear deformation theories (HSDT) [10,14–17] or to Reissner–Mindlin zig-zag interlaminar continuity (RMZC) [1–4,18] formulations have been proposed. The historical reviews on the zig-zag model [1–3] show that three independent approaches, namely Lekhnitskii Multilayered Theory (LMT), Ambartsumian Multilayered Theory (AMT) and Reissner Multilayered Theory (RMT), are available. In the context of the buckling of antisymmetric cross-ply and angle-ply laminates, it is found that true buckling cannot occur in most of the cases [19]. Also, closed-form solutions of the above-mentioned theories can be obtained in only a few cases. Thus, in order to solve a wide class of problems, a numerical scheme such as the finite element method is preferred.

Various finite element models are available for CLPT, FSDT, HSDT, RMZC and other shear deformable theories on composite sandwich plates. Finite element models of the CLPT [9] and HSDT [15,16] with vanishing shear stresses at the top and bottom surfaces of the plates require C^1 continuity. This complicates the development of conforming elements and inhibits their use with other commonly used finite elements. In contrast, finite elements based on FSDT [11], HSDT with polynomial displacement models [20,21] and RMZC [1–4] require only C^0 continuity of all primary variables. Again, both CLPT [9] and FSDTC [11] are inadequate for composite sandwich plates. Hence, to use the finite elements in FSDTV [6,12,13], HSDT with polynomial models [20,21] and RMZC [1–4], a great deal of care is needed to solve the problem with complete confidence. The ideal finite elements [9] to be used in any analysis should converge, not lock, contain no mechanisms, be insensitive to element distortions and be easy to implement and use. One of the popular methods used to develop versatile Mindlin plate elements is the assumed strain concept [22–24]. Most recently, a four-node assumed strain RMZC finite element [1–4] has been used to analyse laminated composite plates. Also, the present authors developed a family of C^0 assumed strain four- and nine-node Lagrange plate finite elements [25–27] based on a refined form of Reddy's higher-order theory which combines FSDTC, FSDTV and third-order theory in a single formulation. From the numerical experiments, it is found that these higher-order elements converge to assumed strain Mindlin plate elements [22–24] by neglecting the in-plane and higher-order terms from the formulation. It can also be stated that both RMZC [1–4]and the present approach [25–27] could be successfully applied to tackle the complex problems in practice. On the vibration of initially stressed sandwich, a finite element model has been developed [28] to validate the experimental results on the natural frequencies and loss factors of initially stressed, damped sandwich beams. A number of finite element formulations based on several theories [1–10,29,30] can be found to analyse buckling and vibration of laminated composite and sandwich panels.

As can be seen from the literature review, apart from the work by Rao et al. [28], the vibration behaviour of composite sandwich plates subjected to various in-plane loads has received very little attention. It can also be observed that the buckling and vibration analysis of initially stressed composite sandwich plates with the use of a family of assumed strain shear deformable finite elements is not attempted so far to the best of the authors' knowledge. In the present study, a new nine-node assumed strain plate bending element is developed based on a refined form of Reddy's higher-order theory by incorporating the terms associated with the geometric stiffness matrix, which is not covered in the earlier analyses [25–27]. Hence, the focus of this paper is a numerical study of the buckling and vibration behaviour of prestressed sandwich plates.

2. Formulation of the problem

The present HSDT [25–27] is developed on the basis of the assumed displacement field in the following form (see Fig. 1):

$$u_\alpha = u_\alpha^0 + z\Psi_\alpha - \frac{4z^3}{3h^2}\phi_\alpha, \quad w = w^0, \tag{1}$$

where the superscript zero denotes the middle surface displacements; Ψ_α are the rotations about the α axes; ϕ_α are the warping functions; h is the thickness of the plate; Greek subscripts range on x and y; u_α are the displacements of a point in the α axes; and w is the displacement in the z-direction. The reason for selecting the displacement field in Eq. (1) is to keep the computing cost minimum in the present analysis. For other forms of HSDT with polynomial models, see Refs. [14,20,21].

The strain–displacement relations of the higher-order theory are obtained from Eq. (1), which can be stated as

$$\varepsilon_{\alpha\beta} = \varepsilon_{\alpha\beta}^0 + z\kappa_{\alpha\beta}^0 + z^3\kappa_{\alpha\beta}^2, \quad \varepsilon_{\alpha\beta}^0 = \frac{1}{2}(u_{\alpha,\beta}^0 + u_{\beta,\alpha}^0), \quad \kappa_{\alpha\beta}^0 = \frac{1}{2}(\Psi_{\alpha,\beta} + \Psi_{\beta,\alpha}),$$

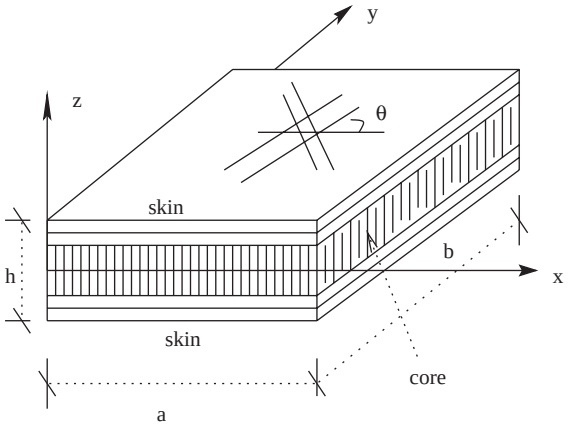

Fig. 1. A typical sandwich plate geometry with laminate reference axes, and fiber orientation.

$$\kappa^2_{\alpha\beta} = \frac{1}{2}\left(\frac{-4}{3h^2}\right)(\Psi_{\alpha,\beta} + \Psi_{\beta,\alpha}),$$

$$\gamma_\alpha = \gamma^s_\alpha + z^2\kappa^s_\alpha, \quad \gamma^s_\alpha = 2\varepsilon_{\alpha z} = w_{,\alpha} + \Psi_\alpha, \quad \kappa^s_\alpha = \left(\frac{-4}{h^2}\right)\phi_\alpha. \tag{2}$$

The stress–strain relations for the lamina in the laminate coordinates (x, y, z) are given by

$$\sigma_{xx} = \overline{Q}_{11}\varepsilon_{xx} + \overline{Q}_{12}\varepsilon_{yy} + 2\overline{Q}_{16}\varepsilon_{xy}, \quad \sigma_{yy} = \overline{Q}_{12}\varepsilon_{xx} + \overline{Q}_{22}\varepsilon_{yy} + 2\overline{Q}_{26}\varepsilon_{xy},$$
$$\sigma_{xy} = \overline{Q}_{16}\varepsilon_{xx} + \overline{Q}_{26}\varepsilon_{yy} + 2\overline{Q}_{66}\varepsilon_{xy}, \quad \sigma_{xz} = 2\overline{Q}_{55}\varepsilon_{xz} + 2\overline{Q}_{54}\varepsilon_{yz}, \quad \sigma_{yz} = 2\overline{Q}_{45}\varepsilon_{xz} + 2\overline{Q}_{44}\varepsilon_{yz}, \tag{3}$$

where $\overline{Q}_{ij}$ are the transformed plane stress reduced elastic stiffness coefficients, which are given as,

$$\begin{aligned}
\overline{Q}_{11} &= Q_{11}c^4 + 2(Q_{12} + 2Q_{66})c^2s^2 + Q_{22}s^4,\\
\overline{Q}_{12} &= (Q_{11} + Q_{22} - 4Q_{66})c^2s^2 + Q_{12}(c^4 + s^4),\\
\overline{Q}_{16} &= (Q_{11}c^2 + (Q_{12} + 2Q_{66})(s^2 - c^2) - Q_{22}s^2)cs,\\
\overline{Q}_{22} &= Q_{11}s^4 + 2(Q_{12} + 2Q_{66})c^2s^2 + Q_{22}c^4,\\
\overline{Q}_{26} &= (Q_{11}s^2 + (Q_{12} + 2Q_{66})(c^2 - s^2) - Q_{22}c^2)cs,\\
\overline{Q}_{66} &= (Q_{11} + Q_{22} - 2Q_{12})c^2s^2 + Q_{66}(c^2 - s^2)^2,
\end{aligned} \tag{4}$$

where $[Q_{ij}]_k$ is the constitutive matrix at lamina level; $c = \cos\theta$; $s = \sin\theta$; θ is the angle between the lamina x-axis and lamina principal x_i-axis. $Q_{11} = E_1/(1 - \nu_{12}\nu_{21})$, $Q_{12} = (\nu_{12}E_2)/(1 - \nu_{12}\nu_{21})$, $Q_{22} = E_2/(1 - \nu_{12}\nu_{21})$, $Q_{66} = G_{12}$, $Q_{55} = G_{13}$, $Q_{44} = G_{23}$ in which E_i is the x_i-axis elastic modulus; ν_{ij} is the i–j plane Poisson ratio; G_{ij} is the i–j plane shear modulus.

The equations of motion associated with the displacement field in Eq. (1) are

$$\begin{aligned}
&N_{xx,x} + N_{xy,y} = I_1\ddot{u}^0_x + I_2\ddot{\Psi}_x + \left(\frac{-4I_4}{3h^2}\right)\ddot{\phi}_x,\\
&N_{xy,x} + N_{yy,y} = I_1\ddot{u}^0_y + I_2\ddot{\Psi}_y + \left(\frac{-4I_4}{3h^2}\right)\ddot{\phi}_y,\\
&Q_{xx,x} + Q_{yy,y} + q + \overline{N}_{xx}w^0_{,xx} + 2\overline{N}_{xy}w^0_{,xy} + \overline{N}_{yy}w^0_{,yy} = I_1\ddot{w}^0,\\
&M_{xx,x} + M_{xy,y} - Q_{xx} = I_2\ddot{u}^0_x + I_3\ddot{\Psi}_x + \left(\frac{-4I_5}{3h^2}\right)\ddot{\phi}_x,\\
&M_{xy,x} + M_{yy,y} - Q_{yy} = I_2\ddot{u}^0_y + I_3\ddot{\Psi}_y + \left(\frac{-4I_5}{3h^2}\right)\ddot{\phi}_y,\\
&\left(\frac{-4}{3h^2}\right)(P_{xx,x} + P_{xy,y}) + \frac{4R_{xx}}{h^2} = \left(\frac{-4I_4}{3h^2}\right)\ddot{u}^0_x + \left(\frac{-4I_5}{3h^2}\right)\ddot{\Psi}_x + \left(\frac{16I_7}{9h^4}\right)\ddot{\phi}_x,\\
&\left(\frac{-4}{3h^2}\right)(P_{xy,x} + P_{yy,y}) + \frac{4R_{yy}}{h^2} = \left(\frac{-4I_4}{3h^2}\right)\ddot{u}^0_y + \left(\frac{-4I_5}{3h^2}\right)\ddot{\Psi}_y + \left(\frac{16I_7}{9h^4}\right)\ddot{\phi}_y.
\end{aligned} \tag{5}$$

The boundary conditions are of the following form:

On the edge with a constant value of x:

$$u_x^0 = \overline{u_x^0} \text{ or } N_{xx} = \overline{N_{xx}}, \quad u_y^0 = \overline{u_y^0} \text{ or } N_{xy} = \overline{N_{xy}}, \quad w^0 = \overline{w^0} \text{ or } Q_{xx} = \overline{Q_{xx}},$$
$$\Psi_x = \overline{\Psi_x} \text{ or } M_{xx} = \overline{M_{xx}}, \quad \Psi_y = \overline{\Psi_y} \text{ or } M_{xy} = \overline{M_{xy}}, \quad \phi_x = \overline{\phi_x} \text{ or } P_{xx} = \overline{P_{xx}},$$
$$\phi_y = \overline{\phi_y} \text{ or } P_{xy} = \overline{P_{xy}}.$$

On the edge with a constant value of y:

$$u_x^0 = \overline{u_x^0} \text{ or } N_{xy} = \overline{N_{xy}}, \quad u_y^0 = \overline{u_y^0} \text{ or } N_{yy} = \overline{N_{yy}}, \quad w^0 = \overline{w^0} \text{ or } Q_{yy} = \overline{Q_{yy}},$$
$$\Psi_x = \overline{\Psi_x} \text{ or } M_{xy} = \overline{M_{xy}}, \quad \Psi_y = \overline{\Psi_y} \text{ or } M_{yy} = \overline{M_{yy}}, \quad \phi_x = \overline{\phi_x} \text{ or } P_{xy} = \overline{P_{xy}},$$
$$\phi_y = \overline{\phi_y} \text{ or } P_{yy} = \overline{P_{yy}}.$$

The various stress resultants are given by

$$\begin{bmatrix} N_{xx} & M_{xx} & P_{xx} \\ N_{yy} & M_{yy} & P_{yy} \\ N_{xy} & M_{xy} & P_{xy} \end{bmatrix} = \sum_{k=1}^{nl} \int_{z_{k-1}}^{z_k} \begin{Bmatrix} \sigma_{xx} \\ \sigma_{yy} \\ \sigma_{xy} \end{Bmatrix} (1, z, z^2)\, \mathrm{d}z, \tag{6a}$$

$$\begin{bmatrix} Q_{xx} & R_{xx} \\ Q_{yy} & R_{yy} \end{bmatrix} = \sum_{k=1}^{nl} \int_{z_{k-1}}^{z_k} \begin{Bmatrix} \tau_{xz} \\ \tau_{yz} \end{Bmatrix} (1, z^2)\, \mathrm{d}z, \tag{6b}$$

where nl is the number of the layer.

Upon simplification, the stress resultants are stated as

$$\begin{aligned} N &= [A]\varepsilon_{\alpha\beta}^0 + [B]\kappa_{\alpha\beta}^0 + [E]\kappa_{\alpha\beta}^2, \\ M &= [B]\varepsilon_{\alpha\beta}^0 + [D]\kappa_{\alpha\beta}^0 + [F]\kappa_{\alpha\beta}^2, \\ P &= [E]\varepsilon_{\alpha\beta}^0 + [F]\kappa_{\alpha\beta}^0 + [H]\kappa_{\alpha\beta}^2, \\ Q &= [A]^s\gamma_\alpha^s + [D]^s\kappa_\alpha^s, \\ R &= [D]^s\gamma_\alpha^s + [F]^s\kappa_\alpha^s, \end{aligned} \tag{6c}$$

where

$$N = (N_{xx} \quad N_{yy} \quad N_{xy})^{\mathrm{T}}, \quad M = (M_{xx} \quad M_{yy} \quad M_{xy})^{\mathrm{T}},$$
$$P = (P_{xx} \quad P_{yy} \quad P_{xy})^{\mathrm{T}}, \quad Q = (Q_{xx} \quad Q_{yy})^{\mathrm{T}}, \quad R = (R_{xx} \quad R_{yy})^{\mathrm{T}},$$
$$(A_{ij}, B_{ij}, D_{ij}, E_{ij}, F_{ij}, H_{ij}) = \sum_{k=1}^{nl} \int_{z_{k-1}}^{z_k} (\overline{Q}_{ij})_k (1, z, z^2, z^3, z^4, z^6)\, \mathrm{d}z, \quad i,j = 1,2,6,$$
$$(A_{ij}^s, D_{ij}^s, F_{ij}^s) = \sum_{k=1}^{nl} \int_{z_{k-1}}^{z_k} (\overline{Q}_{ij})_k (1, z^2, z^4)\, \mathrm{d}z, \quad i,j = 5,4. \tag{7}$$

The inertias I_i $(i = 1, 2, 3, 4, 5, 7)$ are defined by

$$(I_1, I_2, I_3, I_4, I_5, I_7) = \sum_{k=1}^{nl} \int_{z_{k-1}}^{z_k} \rho_k (1, z, z^2, z^3, z^4, z^6)\, \mathrm{d}z, \tag{8}$$

where ρ_k is the material density of the kth layer. In Eq. (5), $\overline{N_{xx}}$, $\overline{N_{yy}}$ and $\overline{N_{xy}}$ denote the constant in-plane edge loads. Both the Navier-type and Levy-type solutions of Eqs. (5) and (6) can be found in Refs. [14,16], respectively.

The principle of virtual work equation can be obtained from Eqs. (5)–(8) in the following form:

$$\begin{aligned}
&\int_0^t \int_A (\delta\varepsilon_{\alpha\beta}^{0\,\mathrm{T}}[A]\varepsilon_{\alpha\beta}^0 + \delta\varepsilon_{\alpha\beta}^{0\,\mathrm{T}}[B]\kappa_{\alpha\beta}^0 + \delta\varepsilon_{\alpha\beta}^{0\,\mathrm{T}}[E]\kappa_{\alpha\beta}^2 + \delta\kappa_{\alpha\beta}^{0\,\mathrm{T}}[B]\varepsilon_{\alpha\beta}^0 + \delta\kappa_{\alpha\beta}^{0\,\mathrm{T}}[D]\kappa_{\alpha\beta}^0 + \delta\kappa_{\alpha\beta}^{0\,\mathrm{T}}[F]\kappa_{\alpha\beta}^2 \\
&\quad + \delta\kappa_{\alpha\beta}^{2\,\mathrm{T}}[E]\varepsilon_{\alpha\beta}^0 + \delta\kappa_{\alpha\beta}^{2\,\mathrm{T}}[F]\kappa_{\alpha\beta}^0 + \delta\kappa_{\alpha\beta}^{2\,\mathrm{T}}[H]\kappa_{\alpha\beta}^2 + \delta\gamma_\alpha^{s\,\mathrm{T}}[A^s]\gamma_\alpha^s + \delta\gamma_\alpha^{s\,\mathrm{T}}[D^s]\kappa_\alpha^s \\
&\quad + \delta\kappa_\alpha^{s\,\mathrm{T}}[D^s]\varepsilon_\alpha^s + \delta\kappa_\alpha^{s\,\mathrm{T}}[F^s]\kappa_\alpha^s)\,\mathrm{d}A\,\mathrm{d}t + \int_0^t \int_A q\,\mathrm{d}w^0\,\mathrm{d}A\,\mathrm{d}t + \int_0^t \int_A [G]^{\mathrm{T}}\overline{[N]}[G]\,\mathrm{d}A\,\mathrm{d}t \\
&\quad = \int_0^t \int_A \Big[I_1(\ddot{u}_x^0\delta u_x^0 + \ddot{u}_y^0\delta u_y^0 + \ddot{w}^0\delta w^0) + I_2(\ddot{\Psi}_x\delta u_x^0 + \ddot{\Psi}_y\delta u_y^0 + \ddot{u}_x^0\delta\Psi_x + \ddot{u}_y^0\delta\Psi_y) \\
&\qquad + \left(\frac{-4I_4}{3h^2}\right)(\ddot{\phi}_x\delta u_x^0 + \ddot{\phi}_y\delta u_y^0 + \ddot{u}_x^0\delta\phi_x + \ddot{u}_y^0\delta\phi_y) \\
&\qquad + \left(\frac{-4I_5}{3h^2}\right)(\ddot{\Psi}_x\delta\phi_x + \ddot{\Psi}_y\delta\phi_y + \ddot{\phi}_x\delta\Psi_x + \ddot{\phi}_y\delta\Psi_y) \\
&\qquad + I_3(\ddot{\Psi}_x\delta\Psi_x + \ddot{\Psi}_y\delta\Psi_y) + \left(\frac{16I_7}{9h^4}\right)(\ddot{\phi}_x\delta\phi_x + \ddot{\phi}_y\delta\phi_y)\Big]\,\mathrm{d}A\,\mathrm{d}t,
\end{aligned} \tag{9}$$

where $[G] = [w_{,x}^0\ w_{,y}^0]^{\mathrm{T}}$ and $\overline{[N]}$ is a matrix containing the inplane edge loads.

3. Finite element approximation

A nine-node isoparametric quadrilateral finite element is developed on the basis of a refined higher-order plate theory as discussed in the previous section. The element displacement function approximations can be expressed as

$$\begin{aligned}
&u_x^0 = \sum_{i=1}^n N_i u_x^{0i}, \quad u_y^0 = \sum_{i=1}^n N_i u_y^{0i}, \quad w^0 = \sum_{i=1}^n N_i w^{0i}, \quad \Psi_x = \sum_{i=1}^n N_i \Psi_x^i, \\
&\Psi_y = \sum_{i=1}^n N_i \Psi_y^i, \quad \phi_x = \sum_{i=1}^n N_i \phi_x^i, \quad \phi_y = \sum_{i=1}^n N_i \phi_y^i,
\end{aligned} \tag{10}$$

where N_i, $i = 1, \ldots, n = 9$, are the interpolation functions. Knowing the generalized displacement vector $(U_{(e)} = [N]^{(e)}\{\delta\}_{(e)})$ at all points within the element 'e', the generalized mid-surface strains at

any point given by Eq. (2) can be expressed in terms of nodal displacements as follows:

$$\varepsilon_{\alpha\beta}^{0(e)} = [B_{\varepsilon}^{0}]^{(e)}\{\delta\}_{(e)}, \quad \kappa_{\alpha\beta}^{0(e)} = [B_{\kappa}^{0}]^{(e)}\{\delta\}_{(e)}, \quad \kappa_{\alpha\beta}^{2(e)} = [B_{\kappa}^{2}]^{(e)}\{\delta\}_{(e)},$$
$$\gamma_{\alpha}^{s(e)} = [B_{\varepsilon}^{s}]^{(e)}\{\delta\}_{(e)}, \quad \kappa_{\alpha}^{s(e)} = [B_{\kappa}^{s}]^{(e)}\{\delta\}_{(e)}, \tag{11}$$

where $[B_{\varepsilon}^{0}]$, $[B_{\kappa}^{0}]$, $[B_{\kappa}^{2}]$, $[B_{\varepsilon}^{s}]$ and $[B_{\kappa}^{s}]$ are generated strain–displacement matrices.

One basic problem associated with the use of standard interpolation of the strains for the transverse shear components is that the element locks when it is thin. The reason for this locking is that the element, when loaded in pure bending, will exhibit spurious transverse shear energy. In order to overcome the shear locking, Huang and Hinton [23] proposed assumed interpolations for the shear strain to develop a nine-node assumed strain Mindlin plate bending element. In this paper, the same interpolation scheme is used to develop the nine-node plate bending element based on a refined higher-order theory. According to the Kirchhoff–Love hypothesis, the shear strains are insignificant in thin plate situations. Hence, the following conditions should apply in both global and local coordinate systems:

$$\gamma_{\alpha}^{s} = \begin{bmatrix} \gamma_{xz} \\ \gamma_{yz} \end{bmatrix} = \begin{bmatrix} \Psi_x + w_{,x} \\ \Psi_y + w_{,y} \end{bmatrix} ----> 0, \tag{12}$$

$$\begin{bmatrix} \gamma_{\xi\zeta} \\ \gamma_{\eta\zeta} \end{bmatrix} = \begin{bmatrix} \Psi_{\xi} + w_{,\xi} \\ \Psi_{\eta} + w_{,\eta} \end{bmatrix} ----> 0. \tag{13}$$

The polynomial terms for Ψ_{ξ}, $w_{,\xi}$, Ψ_{η} and $w_{,\eta}$ in a nine-node Lagrange element are given by

$$\begin{aligned} \Psi_{\xi} &= f(1, \xi, \eta, \xi\eta, \xi^2, \eta^2, \xi^2\eta, \xi\eta^2, \xi^2\eta^2), \\ w_{,\xi} &= f(1, \xi, \eta, \xi\eta, \eta^2, \xi\eta^2), \\ \Psi_{\eta} &= f(1, \xi, \eta, \xi\eta, \xi^2, \eta^2, \xi^2\eta, \xi\eta^2, \xi^2\eta^2), \\ w_{,\eta} &= f(1, \xi, \eta, \xi\eta, \xi^2, \xi^2\eta). \end{aligned} \tag{14}$$

From Eq. (14), it is seen that the terms for Ψ_{ξ} and $w_{,\xi}$ and for Ψ_{η} and $w_{,\eta}$ do not match. Hence, the substitute strain fields [23] are introduced as

$$\begin{aligned} \overline{\gamma}_{\xi\zeta} &= p_1 + p_2\xi + p_3\eta + p_4\xi\eta + p_5\eta^2 + p_6\xi\eta^2, \\ \overline{\gamma}_{\eta\zeta} &= q_1 + q_2\xi + q_3\eta + q_4\xi\eta + q_5\xi^2 + q_6\xi^2\eta. \end{aligned} \tag{15}$$

A constrained functional [23] is introduced to replace the total potential energy (Π) expression as

$$\overline{\Pi} = \Pi + \int_A \lambda^{13}(\overline{\gamma}_{\xi\zeta} - \gamma_{\xi\zeta})\,\mathrm{d}A + \int_A \lambda^{23}(\overline{\gamma}_{\eta\zeta} - \gamma_{\eta\zeta})\,\mathrm{d}A, \tag{16}$$

where λ^{13} and λ^{23} are Lagrangian multipliers. The substitute shear strain fields [23,24] are chosen as

$$\overline{\gamma}_{\xi\zeta} = \sum_{i=1}^{2}\sum_{j=1}^{3} P_i(\xi)Q_j(\eta)\overline{\gamma}_{\xi\zeta}^{ij},$$

$$\overline{\gamma}_{\eta\zeta} = \sum_{i=1}^{3}\sum_{j=1}^{2} Q_i(\xi)P_j(\eta)\overline{\gamma}_{\eta\zeta}^{ji},$$

where

$$Q_1(z) = z(1+z)/2, \quad Q_2(z) = (1-z^2), \quad Q_3(z) = z(z-1)/2,$$
$$P_1(z) = (1+z/s)/2, \quad P_2(z) = (1-z/s)/2, \quad (z = \xi, \eta), \tag{17}$$

in which $s = 0.577$, $\overline{\gamma}_{\xi\zeta}^{ij}$ and $\overline{\gamma}_{\eta\zeta}^{ji}$ are the $m \times n$ unknown substitute shear strain parameters associated with two sets of $m \times n$ sampling points $(\hat{\xi}_i, \hat{\eta}_j)$ and $(\check{\xi}_j,\ \check{\eta}_i)$ (see Fig. 2 for location of sampling points).

In order to eliminate locking, the following equations are obtained:

$$\overline{\gamma}_{\xi\zeta}(\hat{\xi}_i, \hat{\eta}_j) = \gamma_{\xi\zeta}(\hat{\xi}_i, \hat{\eta}_j), \quad i = 1, \ldots, m;\ j = 1, \ldots, n, \tag{18}$$

$$\overline{\gamma}_{\eta\zeta}(\check{\xi}_j, \check{\eta}_i) = \gamma_{\eta\zeta}(\check{\xi}_j, \check{\eta}_i), \quad i = 1, \ldots, n;\ j = 1, \ldots, m. \tag{19}$$

The tensor transformation is used to get $\overline{\gamma}_{xz}$ and $\overline{\gamma}_{yz}$ from $\overline{\gamma}_{\xi\zeta}$ and $\overline{\gamma}_{\eta\zeta}$, respectively, as given by Eq. (17). For further details, see Refs. [23,24]. For implementation purpose, γ_α^s in Eq. (9) is replaced by $\overline{\gamma}_\alpha^s$, where $\overline{\gamma}_\alpha^s$ is the substitute shear strains to remove spurious zero energy modes. Hence, the substitute shear strain $\overline{\gamma}_\alpha^s$ is given by

$$\overline{\gamma}_\alpha^{s(e)} = [\overline{B}_\varepsilon^s]^{(e)}\{\delta\}_{(e)}, \tag{20}$$

where $[\overline{B}_\varepsilon^s]^{(e)}$ is generated strain–displacement matrix.

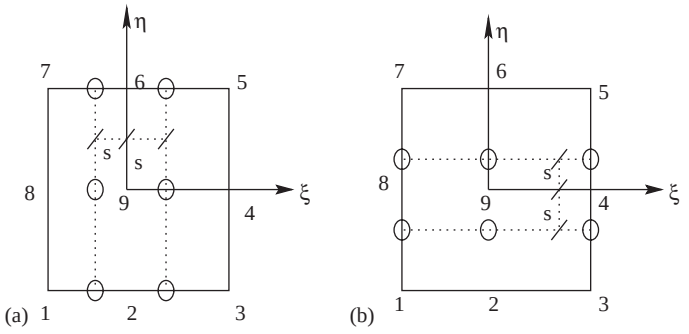

Fig. 2. Location of sampling points for shear interpolation in a nine-node assumed strain element (a) $\overline{\gamma}_{\xi\zeta}^{ij}$ and (b) $\overline{\gamma}_{\eta\zeta}^{ji}$; $s = 0.577$.

For arbitrary value of virtual displacements, Eq. (9) finally leads to the following assembled equations:

$$[M]\{\ddot{\Delta}\} + [K]\{\Delta\} = \{F\} + \lambda_b[K_g]\{\Delta\}. \tag{21}$$

Here the unknown vector $\{\Delta\}$ is generated by the assemblage of element degrees of freedom $\{d\}_e^{\mathrm{T}}, e = 1, \ldots,$ total degrees of freedom in the region **R**. λ_b denotes the buckling parameter (a function of the constant in-plane edge loads $\overline{N}_{xx}$, $\overline{N}_{yy}$ or $\overline{N}_{xy}$). The assembled stiffness, mass and buckling matrices for vibration and buckling analysis are

$$\begin{aligned}[K] = \sum_e \int_{A_e} & [[B_\varepsilon^0]^{\mathrm{T}}[A][B_\varepsilon^0] + [B_\varepsilon^0]^{\mathrm{T}}[B][B_\kappa^0] + [B_\varepsilon^0]^{\mathrm{T}}[E][B_\kappa^2] + [B_\kappa^0]^{\mathrm{T}}[B][B_\varepsilon^0] + [B_\kappa^0]^{\mathrm{T}}[D][B_\kappa^0] \\ & + [B_\kappa^0]^{\mathrm{T}}[F][B_\kappa^2] + [B_\kappa^2]^{\mathrm{T}}[E][B_\varepsilon^0] + [B_\kappa^2]^{\mathrm{T}}[F][B_\kappa^0] + [B_\kappa^2]^{\mathrm{T}}[H][B_\kappa^2] + [\overline{B}_\varepsilon^s]^{\mathrm{T}}[A^s][\overline{B}_\varepsilon^s] \\ & + [\overline{B}_\varepsilon^s]^{\mathrm{T}}[D^s][B_\kappa^s] + [B_\kappa^s]^{\mathrm{T}}[D^s][\overline{B}_\varepsilon^s] + [B_\kappa^s]^{\mathrm{T}}[F^s][B_\kappa^s]]\,\mathrm{d}A,\end{aligned} \tag{22}$$

$$[M] = \sum_e \int_{A_e} [N]^{\mathrm{T}}[M_I][N]\,\mathrm{d}A, \tag{23}$$

$$[K_g] = \sum_e \int_{A_e} [X]^{\mathrm{T}}[\overline{N}][X]\,\mathrm{d}A, \tag{24}$$

where $[X] = [N_{,x}\ N_{,y}]^{\mathrm{T}}$, $[M_I]$ is the mass matrix containing inertia terms and $\{F\}$ is the column vector containing the boundary and body force contributions.

A 3×3 Gauss–Legendre rule (i.e. full integration scheme) is employed to integrate bending, membrane, shear and inertia terms in the energy expressions for the nine-node element.

4. Numerical results and discussions

Numerical results are presented to evaluate the performance characteristics of the newly developed plate bending element in the buckling and free vibration analysis of initially stressed composite sandwich plates. Validation studies on isotropic and laminated composite are undertaken before carrying out sandwich plate analysis. The following boundary conditions are adopted the analysis: Simply supported (S) (for cross ply): $u_x^0 = w^0 = \Psi_x = \phi_x = 0$ at $y = 0, b$; $u_y^0 = w^0 = \Psi_y = \phi_y = 0$ at $x = 0, a$; (S) (for angle ply): $u_y^0 = w^0 = \Psi_x = \phi_x = 0$ at $y = 0, b$; $u_x^0 = w^0 = \Psi_y = \phi_y = 0$ at $x = 0, a$; Clamped (C): $u_x^0 = u_y^0 = w^0 = \Psi_x = \phi_x = \Psi_y = \phi_y = 0$ at $x = 0, a$ and $y = 0, b$.

Firstly, a stability analysis is carried out on isotropic simply supported square plates ($v = 0.30$) to investigate the convergence of the present plate bending element. Table 1 compares the present results on critical buckling loads ($\overline{N} = \overline{N}_{xx}a^2/\pi^2 D$; $D = Eh^3/12(1 - v^2)$), for $a/h = 5$–100 with the analytical solution [15]. From the results, it can be concluded that the present results converge towards the analytical solutions on the refinement of the mesh densities in the full plate.

The natural frequencies $(\omega^2\rho h a^4/D)^{1/2}$ of a clamped square plate (isotropic) under biaxial tension $\overline{N}_{xx}a^2/\pi^2 D(\overline{N}_{xx} = \overline{N}_{yy})$, where D is $Eh^3/12(1 - v^2)$, are later considered to check the numerical accuracy of the approach. The results from three mesh sizes (4×4, 6×6, 8×8) in the full

Table 1
Convergence of critical buckling loads $\overline{N} = \overline{N}_{xx}a^2/\pi^2 D$ for a simply supported square plate under uniaxial compression

Source	Nodes per side	a/h				
		5	10	20	50	100
Present	9	3.2676	3.7896	3.9477	3.9941	4.0002
	13	3.2658	3.7872	3.9450	3.9912	3.9975
	17	3.2656	3.7867	3.9445	3.9901	3.9939
Analytical [15]	—	3.2653	3.7865	3.9443	3.9909	3.9977

Table 2
The natural frequencies $(\omega^2\rho h a^4/D)^{1/2}$ for a clamped square plate under biaxial tension

Source	Mesh	$\overline{N}_{xx}a^2/\pi^2 D$		
		5	10	30
Present	(4×4)	49.608	59.936	89.259
	(6×6)	49.551	59.887	89.209
	(8×8)	49.540	59.878	89.202
Dickinson [31]		49.580	59.925	89.272

Table 3
Convergence of the normalized critical buckling loads $\overline{N} = \overline{N}_{xx}a^2/h^3 E_2$ for a simply supported square bidirectional composite plates (0/90/90/0) with $a/h = 10$ under uniaxial compression

Nodes per side	(E_1/E_2)[a]	
	20	40
5	1.030	1.029
9	1.019	1.019
13	1.018	1.019

[a]Exact solutions [12] for $E_1/E_2 = 20$ and 40 are 15.0191 and 22.8807, respectively.

plate are compared with the analytical solution [31] in Table 2. From the results, it can be inferred that the present solutions are in excellent agreement with the series solution [31]. The frequency increases with an increase in the stiffness of the plate as expected.

Again, a convergence study is carried out on the stability analysis of laminated composite square plates with cross-ply lay-up (0/90/90/0). The material and geometry of the square plate considered here are [12]: $E_1/E_2 = 40$, $G_{12}/E_2 = G_{13}/E_2 = 0.6$, $G_{23}/E_2 = 0.5$, $\nu_{12} = 0.25$ and $a/h = 10$. The present results from full plate discretization with 5, 9 and 13 nodes per side are normalized with exact solution [12] in Table 3. The present finite element formulation gives results within 2% of the exact solution on refinement of mesh sizes as seen from the results.

Table 4
Effect of the degree of orthotropy on critical buckling loads $\overline{N} = \overline{N}_{xx}a^2/h^3E_2$ for a simply supported square bidirectional symmetric composite plates with $a/h = 10$ under uniaxial compression

Source	Number of layers	E_1/E_2				
		3	10	20	30	40
Present	3	5.3905	9.8336	14.8906	18.8778	22.1194
Exact [12]		5.3044	9.7621	15.0191	19.3040	22.8807
HSDT [17]		5.3933	9.9406	15.2980	19.6740	23.3400
CLPT [17]		5.7538	11.4920	19.7120	27.9360	36.160
Present	5	5.4072	10.0828	15.7555	20.5078	24.5588
Exact [12]		5.3255	9.9603	15.6527	20.4663	24.5929
HSDT [17]		5.4096	10.1500	16.0080	20.9990	25.3080
CLPT [17]		5.7538	11.4920	19.7120	27.9360	36.1600
Present	9	5.4126	10.1732	16.0807	21.1341	25.5112
Exact [12]		5.3352	10.0417	15.9153	20.9614	25.3436
HSDT [17]		5.4313	10.1970	16.1720	21.3150	25.7900
CLPT [17]		5.7538	11.4920	19.7120	27.9360	36.1600

In order to study the effect of individual layers on the critical buckling loads of symmetric composite laminates, a finite element mesh (6×6) in a full plate is employed. The following dimensionless orthotropic material properties (typical of high-modulus graphite-epoxy) are used [12]: $E_1/E_2 =$ variable, $G_{12}/E_2 = G_{13}/E_2 = 0.6$, $G_{23}/E_2 = 0.5$ and $\nu_{12} = 0.25$. The present results are compared with exact solution [12], HSDT [17] and CLPT [17] in Table 4. It is seen that the present results are in very good agreement with the exact [12] and analytical solutions [17]. As expected, the CLPT overpredicts critical buckling loads for thick plates ($a/h = 10$). The shear deformation effect is more pronounced for a material with a high degree of anisotropy as seen from the increasing buckling loads with an increase of E_1/E_2 ratios.

The validation problem on sandwich panels includes simply supported square sandwich plates $[0/90/0/90/0/\text{core}]_s$ with the following material characteristics [32]: Face sheets: $E_L/E_T = 19$, $G_{LT}/E_T = 0.52$, $G_{TT}/E_T = 0.338$, $\nu_{LT} = 0.32$, $\nu_{TT} = 0.49$. Honeycomb titanium core: $E_1/E_T = 3.2 \times 10^{-5}$, $E_2/E_T = 2.9 \times 10^{-5}$, $E_3/E_T = 0.4$, $G_{12}/E_T = 2.4 \times 10^{-3}$, $G_{13}/E_T = 7.9 \times 10^{-2}$, $G_{23}/E_T = 6.6 \times 10^{-2}$, $\nu_{12} = 0.99$, $\nu_{13} = \nu_{23} = 3 \times 10^{-5}$, where subscript L is the direction of fibers, T is the transverse direction, subscripts 1,2,3 = the x, y and z directions; ν_{LT} = the major Poisson's ratio. From the numerical experiments, it is found that the results from a mesh of 13 nodes per side in a full plate give satisfactory solutions for sandwich problems. The present results along with exact solution [32] are shown in Table 5 for $a/h = 10$ and 20 with $2h_f/h$ varied between 0.05 and 0.2, where h_f is the thickness of the face sheets. It can be concluded that the present results are in excellent agreement with the exact solution.

Based on the foregoing convergence and validation studies, it can be concluded that the present finite element solutions give reliable results for isotropic, laminated and composite sandwich plate

Table 5
Critical buckling stresses ($\sigma_r a^2/E_T h^2$) for uniaxially loaded, simply supported composite sandwich plates

Source	Nodes per side	$2h_f/h$			
		0.05	0.10	0.15	0.20
		$a/h = 10$			
Present	13	2.2940	3.8540	4.9690	5.8080
Exact [32]		2.2081	3.7385	4.8307	5.6721
		$a/h = 20$			
Present	13	2.5761	4.7160	6.5044	8.0086
Exact [32]		2.5534	4.6460	6.4401	7.9352

problems. For the remaining problems, a 6×6 mesh in full plate will be considered. The structural sandwiches considered in the remaining studies have square planform with face sheets of 8 plies of Graphite/Epoxy (GE) placed symmetrically about a poly-vinyl chloride (PVC) foam core. The material characteristics of the face sheets and the core are given by: Face sheets [27]: $E_L = 128\,\text{GPa}$, $E_T = 11.0\,\text{GPa}$, $v_{LT} = 0.25$, $G_{LT} = 4.48\,\text{GPa}$, $G_{13} = 4.48\,\text{GPa}$, $G_{23} = 1.53\,\text{GPa}$, $\rho_f = 1.5 \times 10^3\,\text{kg/m}^3$. HEREX C70.130 Core [27]: $E_c = 103.63\,\text{MPa}$, $G_c = 50\,\text{MPa}$, $v_c = 0.32$, $\rho_c = 130\,\text{kg/m}^3$.

This example involves the effect of face thickness to overall thickness ratio on the critical buckling stress and fundamental frequency of initially stressed composite sandwich plate. Sandwich panels are assumed to be simply supported under uniaxial stress fields. The results from the present formulation are shown in Fig. 3(a). For panels with $h/a = 0.05$–0.20, as the thickness ratio of the face sheets, $2h_f/h$ increases from 0.05 to 0.2, the critical compressive stress ($\sigma_r a^2/E_T h^2$) increases. The reason for the increase in the critical buckling stress is due to the contribution from the stiff face sheets to resist more in-plane loads. After determining the critical buckling stress, a series of vibration analyses are carried out to determine the fundamental frequency $(\omega^2 \rho_f a^4/E_T h^2)^{1/2}$ of the square plate with $a/h = 10$ under in-plane stresses expressed as a fraction of the critical buckling stress. The results are shown in Fig. 3(b) which shows that as the in-plane stress approaches the buckling stress, the frequency of the plate decreases to zero. For panels with $h/a = 0.10$, as the thickness ratio of the face sheets, $2h_f/h$, increases from 0.05 to 0.2, the fundamental frequency decreases. As the plate becomes heavier in weight, the frequency value decreases. Thus, there is a trade-off between stiffness, buckling and mass effects on the fundamental frequency.

This example deals with the effect of stacking sequence on the buckling and free vibration of uniaxially stressed simply supported composite sandwich plates. Three stacking sequences $[0/0/0/0/\text{core}]_s$, $[0/45/-45/90/\text{core}]_s$ and $[0/90/0/90/\text{core}]_s$ are taken. As seen in Fig. 4(a), for $a/h = 10$, and $2h_f/h$ from 0.05 to 0.20, the buckling stress increases with the increase of $2h_f/h$. Thus, the stiffer plate offers higher buckling stress. The sandwich plate with $[0/0/0/0/\text{core}]_s$ shows higher buckling stress than $[0/90/0/90/\text{core}]_s$ and $[0/45/-45/90/\text{core}]_s$. This is due to the applied in-plane load is in the longitudinal direction of the fibers (stronger) in the sandwich plate with $[0/0/0/0/\text{core}]_s$. This shows that the stacking sequence effects the critical buckling stress in a

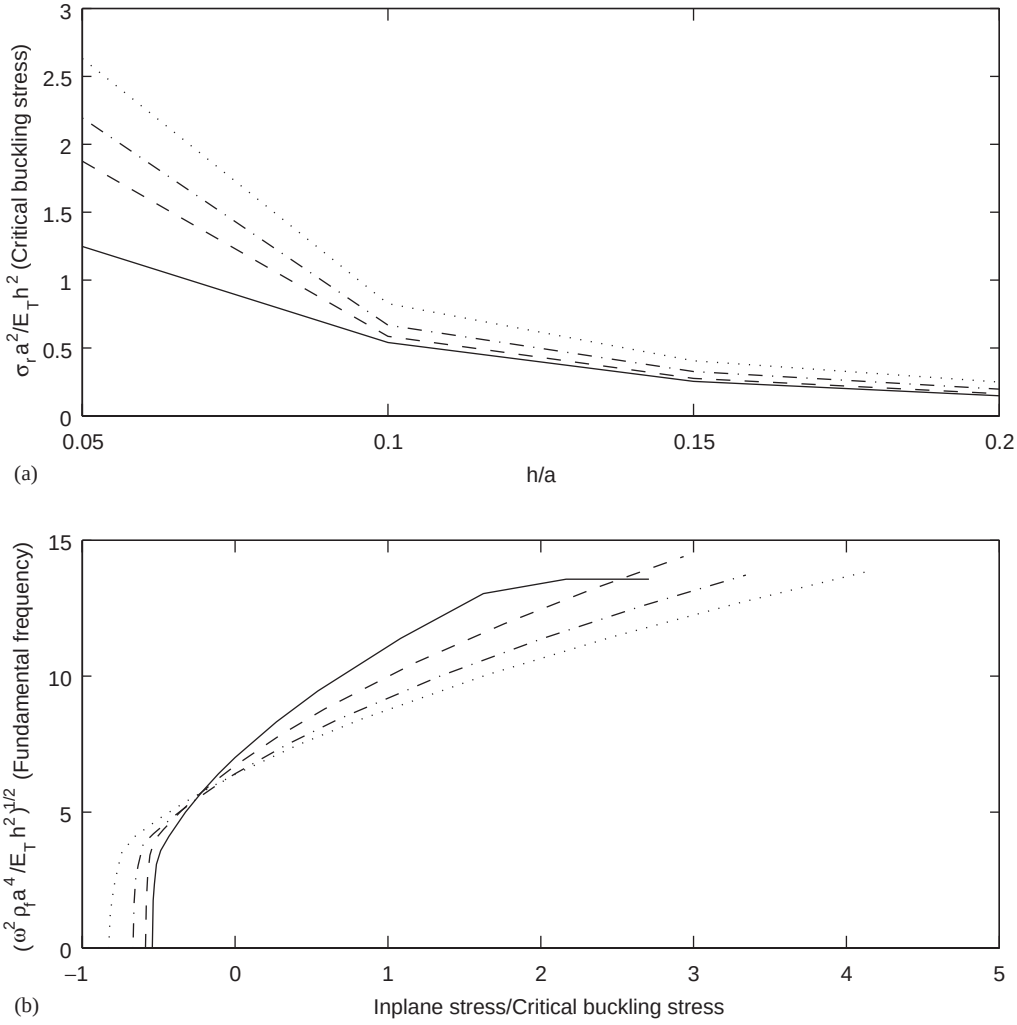

Fig. 3. Effect of thickness ratios on (a) critical buckling stresses ($\sigma_r a^2/E_T h^2$) and (b) fundamental frequencies ($(\omega^2\rho_f a^4/E_T h^2)^{1/2}$) of composite sandwich plates; —— $2h_f/h = 0.05$, − − − − $2h_f/h = 0.10$, −. − . − $2h_f/h = 0.15$, ... $2h_f/h = 0.20$.

composite sandwich plate than isotropic plates. The designer can get the desired buckling stresses by varying the stacking sequence in a composite sandwich plate. Again the natural frequencies $(\omega^2\rho_f a^4/E_T h^2)^{1/2}$ for a square plate with $a/h = 10$ and $2h_f/h = 0.20$ are determined under a series of in-plane buckling stresses as shown in Fig. 4(b). Similarly, the fundamental frequencies show increasing trend with the increase of critical buckling stresses. The positive critical buckling stress denotes the tensile stress which increases the stiffness of the plate. Hence, the presence of tensile stresses increases the fundamental frequencies in the present case.

This example includes the effect of boundary conditions on the critical buckling stress and fundamental frequencies of uniaxially stressed composite sandwich plates. The results from the

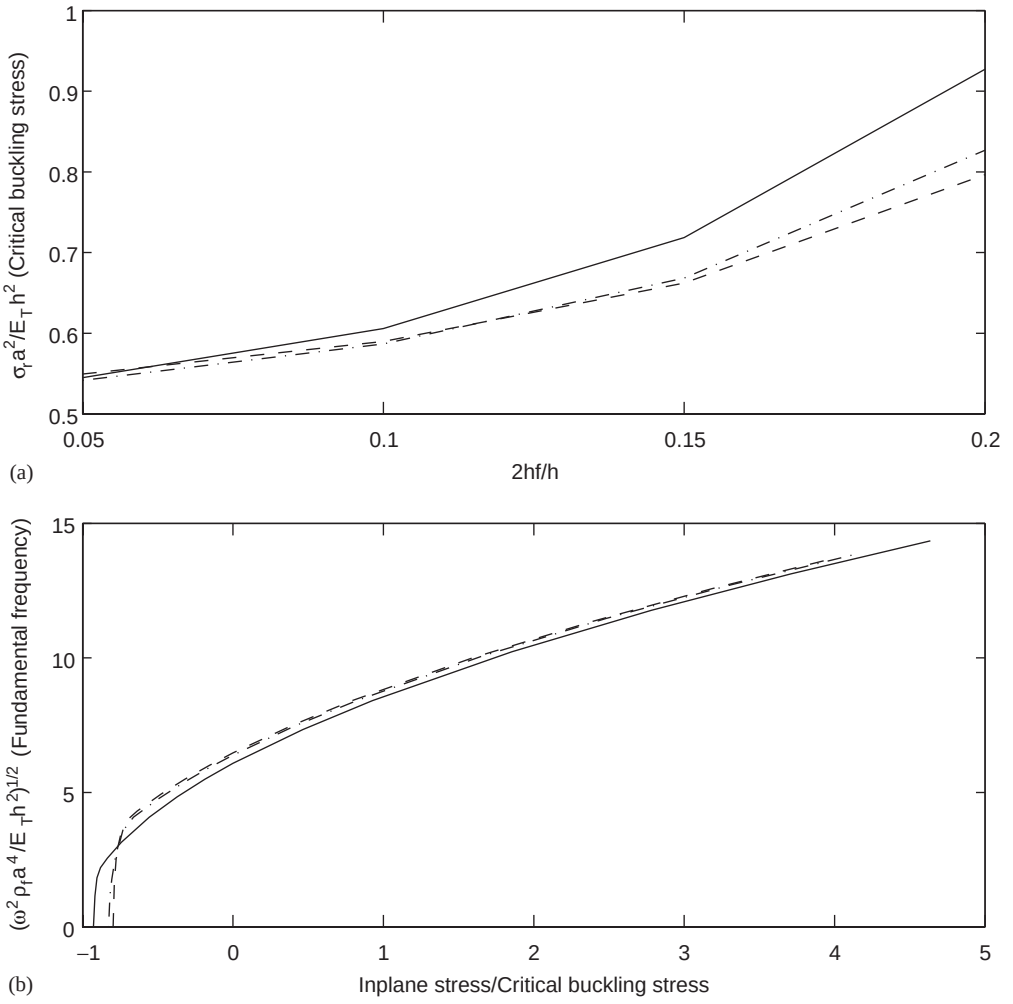

Fig. 4. Effect of stacking sequence on (a) critical buckling stresses ($\sigma_r a^2/E_T h^2$) and (b) fundamental frequencies ($(\omega^2\rho_f a^4/E_T h^2)^{1/2}$) of composite sandwich plates; —— [0/0/0/0/core/0/0/0/0], – – – – [0/45/ − 45/90/core/90/ −45/45/0], −. − . − [0/90/0/90/core/90/0/90/0].

present formulation are shown in Fig. 5(a) for composite sandwich plates under in-plane edge loads. The boundary conditions *SSSS*, *CCCC*, *CFFF*, *CFCF* and *CSCS* denote the sides ($y = 0$ and $x = 0$–a, $x = a$ and $y = 0$–a, $y = a$ and $x = 0$–a, $x = 0$ and $y = 0$–a) where *S*, *C* and *F* indicate simply supported, clamped and free edge conditions. From Fig. 5(a), it is seen that *CCCC* has highest buckling load among all the boundary conditions, which is about 5 to 7 times higher than its *CFFF* counterpart, depending on the plate thickness ratios ($2h_f/h$). It can also be observed that the critical buckling stress ($\sigma_r a^2/E_T h^2$) increases with the increase of $2h_f/h$. The reason may be due to the coupling effects between the membrane, bending and shear terms contributed from GE material in the skin. Hence, the stiff plates should be analysed carefully for stability considerations. Again the fundamental frequencies $(\omega^2\rho_f a^4/E_T h^2)^{1/2}$ for a square plate

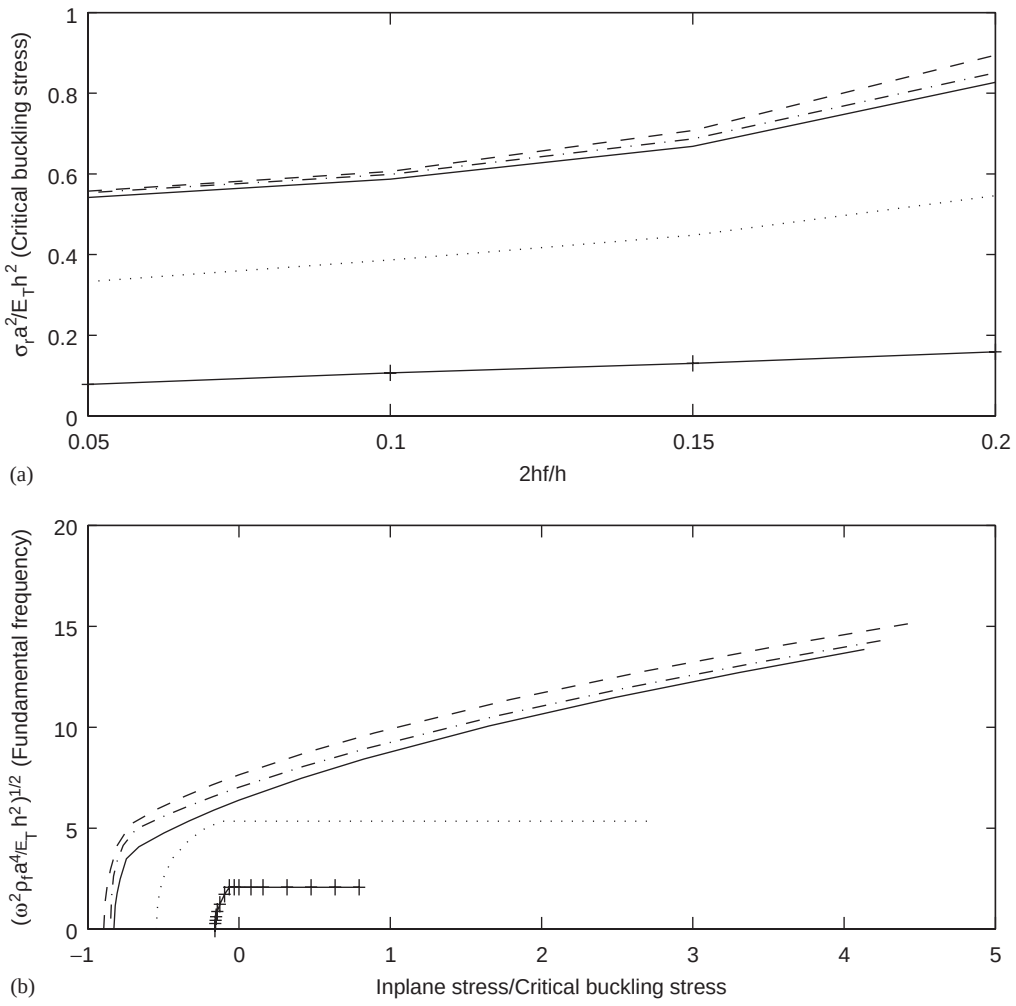

Fig. 5. Effect of boundary conditions on (a) critical buckling stresses ($\sigma_r a^2/E_T h^2$) and (b) fundamental frequencies ($(\omega^2\rho_f a^4/E_T h^2)^{1/2}$) of composite sandwich plates; —— *SSSS*, − − − − *CCCC*, −. − . − *CSCS*, ... *CFCF*, − + − + − *CFFF*.

with $a/h = 10$ and $2h_f/h = 0.20$ are determined under a series of in-plane buckling stresses as shown in Fig. 5(b). *CFFF* and *CFCF* do not show any increase in fundamental frequencies under tensile stresses. The reason may be that the free edges are loaded in tension, without contributing much to stability matrix.

In the last example, the effect of various in-plane loads on the critical buckling stresses and fundamental frequency of composite sandwich plates is investigated. The composite sandwich plate is simply supported with $a = b$, $a/h = 10$ and $2h_f/h = 0.05$. The results from the present investigation are shown in Fig. 6(a) for buckling stresses ($\sigma_r a^2/E_T h^2$) depending on the types of in-plane loads applied to the sandwich panel. The inplane loads are classified into uniaxial compressive stress in x-direction (Uniaxial-x), Uniform shear (Shear), Biaxial compressive stresses

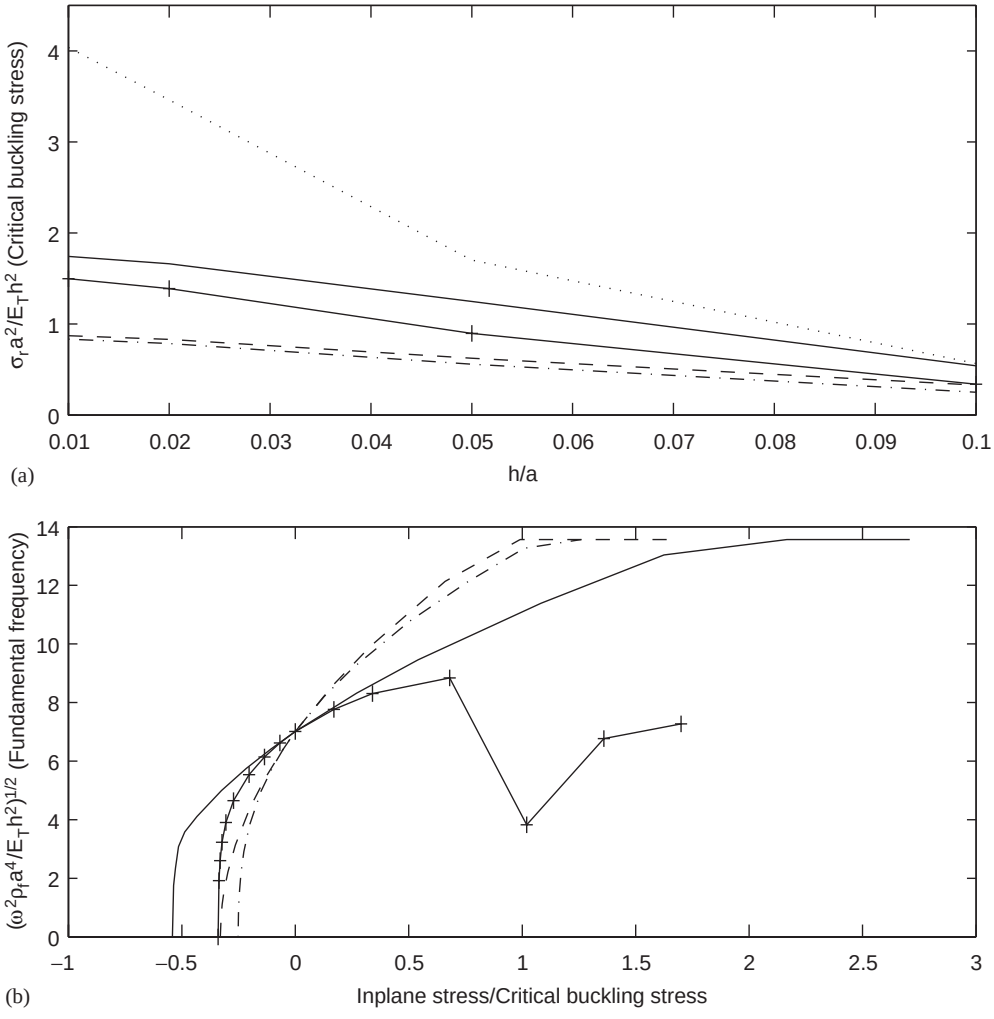

Fig. 6. Effects of various inplane stresses on (a) critical buckling stresses ($\sigma_r a^2/E_T h^2$) and (b) fundamental frequencies ($(\omega^2\rho_f a^4/E_T h^2)^{1/2}$) of composite sandwich plates; —— Uniaxial-x, − − − − Biaxial, −.−.− Combined, −+−+ Uniaxial-x and shear, ... Shear.

(Biaxial), Uniaxial compression in x-direction and shear (Uniaxial-x and Shear) and Combination of biaxial compression and Shear (Combined). The effects of various thickness to side ratios on critical buckling stresses are also shown in Fig. 6(a). As expected, the critical buckling stress in sandwich panels under shear is the highest among all inplane stresses, which is also true as that for isotropic plates. The composite sandwich plate under combined loading gives the lowest critical buckling stresses. The reason is the coupling effects between compressive and shear loads on the sandwich panels. Also, the thinner plates possess higher buckling loads than thicker plates, which is also the same as that of isotropic plates, as seen in Example 1. Again, the fundamental frequencies $(\omega^2\rho_f a^4/E_T h^2)^{1/2}$ for a square plate with $a/h = 10$ and $2h_f/h = 0.05$ are determined

under a series of in-plane buckling stresses as shown in Fig. 6(b). The fundamental frequencies show increasing trend with the increase of critical buckling stresses except for Uniaxial-x and shear stresses. In case of Uniaxial-x and shear, the fundamental frequency shows increasing trend up to 2 times of the critical buckling stress. The change in fundamental frequency shows the damage in the panel under tensile stresses and shear stresses, which are 3 times of the critical buckling stresses.

5. Closure

In this paper, a shear deformable plate bending element is developed based on a refined third-order theory to analyse buckling and free vibration of initially stressed composite sandwich plates. An assumed strain concept is applied to remove shear locking and spurious zero energy modes in the finite element formulation. A consistent mass matrix is incorporated to preserve the total kinetic energy of the system. Full integration rather than uniform reduced integration is carried out along with the assumed strain concept to integrate various terms in the energy expressions. The developed nine-node plate bending element is validated for isotropic, laminated and composite sandwich plates for generic validation studies. Several examples are presented to show the effects of parameters like thickness ratios, stacking sequence, boundary conditions and types of inplane loads on the critical buckling stresses and fundamental frequencies.

References

[1] E. Carrera, Historical review of zig-zag theories for multilayered plates and shells, *Applied Mechanics Reviews* 56 (2003) 287–308.
[2] E. Carrera, Theories and finite elements for multilayered, anisotropic, composite plates and shells, *Archives of Computational Methods in Engineering* 9 (2002) 87–140.
[3] E. Carrera, Theories and finite elements for multilayered plates and shells: a unified compact formulation with numerical assessment and benchmarking, *Archives of Computational Methods in Engineering* 10 (2003) 215–296.
[4] E. Carrera, L. Demasi, Two benchmarks to assess two dimensional theories of sandwich composite plates, *AIAA Journal* 41 (2003) 1356–1362.
[5] J.R. Vinson, Sandwich structures, *Applied Mechanics Reviews* 54 (2001) 201–214.
[6] A.K. Noor, W.S. Burton, C.W. Bert, Computational models for sandwich panels and shells, *Applied Mechanics Reviews* 49 (1996) 155–199.
[7] J.N. Reddy, D.H. Robbins Jr., Theories and computational models for composite laminates, *Applied Mechanics Reviews* 47 (1994) 147–169.
[8] J. Mackerle, Finite element analyses of sandwich structures: a bibliography (1980–2001), *Engineering Computations* 19 (2002) 206–245.
[9] H.T.Y. Yang, S. Saigal, A. Masud, R.K. Kapania, A survey of recent shell finite elements, *International Journal for Numerical Methods in Engineering* 47 (2000) 101–127.
[10] Mallikarjuna, T. Kant, A critical review and some results of recently developed refined theories of fiber-reinforced laminated composites and sandwiches, *Composite Structures* 23 (1993) 293–312.
[11] M. Ganapathi, O. Polit, M. Touratier, A C^0 eight-node membrane-shear-bending element for geometrically non-linear (static-dynamic) analysis of laminates, *International Journal for Numerical Methods in Engineering* 39 (1996) 3453–3474.
[12] A.K. Noor, Stability of multilayered composite plates, *Fiber Science and Technology* 8 (1975) 81–89.

[13] R. Rikards, A. Chate, A. Korjakin, Vibration and damping analysis of laminated composite plates by the finite element method, *Engineering Computations* 12 (1995) 61–74.
[14] T. Kant, K. Swaminathan, Analytical solutions using a higher order refined theory for the stability analysis of laminated composite and sandwich plates, *Structural Engineering and Mechanics* 10 (2000) 337–357.
[15] J.N. Reddy, N.D. Phan, Stability and vibration of isotropic, orthotropic and laminated plates according to a higher-order shear deformation theory, *Journal of Sound and Vibration* 98 (1985) 157–170.
[16] A.A. Khdeir, Free vibration and buckling of symmetric cross-ply laminated plates by an exact method, *Journal of Sound and Vibration* 126 (1988) 447–461.
[17] N.S. Putcha, J.N. Reddy, Stability and natural vibration analysis of laminated plates by using a mixed element based on a refined plate theory, *Journal of Sound and Vibration* 104 (1986) 285–300.
[18] E. Carrera, A refined multi-layered finite element model applied to linear and non-linear analysis of sandwich plates, *Composite Science and Technology* 58 (1998) 1553–1569.
[19] M.S. Qatu, A.W. Leissa, Buckling or transverse deflections of unsymmetrically laminated plates subjected to in-plane loads, *AIAA Journal* 31 (1993) 189–194.
[20] C.S. Babu, T. Kant, Two shear deformable finite element models for buckling analysis of skew fiber-reinforced composite and sandwich panels, *Composite Structures* 46 (1999) 115–124.
[21] J.S. Moita, C.M.M. Soares, C.A.M. Soares, Buckling and dynamic behaviour of laminated composite structures using a discrete higher-order displacement model, *Computers and Structures* 73 (1999) 407–423.
[22] E.N. Dvorkin, K.J. Bathe, A continuum mechanics based four node shell element for general nonlinear analysis, *Engineering Computations* 1 (1984) 77–88.
[23] H.C. Huang, E. Hinton, A nine node Lagrangian Mindlin plate element with enhanced shear interpolation, *Engineering Computations* 1 (1984) 369–379.
[24] E. Hinton, H.C. Huang, A family of quadrilateral Mindlin plate elements with substitute shear strain fields, *Computers and Structures* 23 (1986) 409–431.
[25] A.K. Nayak, S.S.J. Moy, R.A. Shenoi, Free vibration analysis of composite sandwich plates based on Reddy's higher-order theory, *Composites Part B: Engineering* 33 (2002) 505–519.
[26] A.K. Nayak, R.A. Shenoi, S.S.J. Moy, Analysis of damped composite sandwich plates using plate bending elements with substitute shear strain fields based on Reddy's higher-order theory, *Journal of Mechanical Engineering Sciences* 216 (2002) 591–606.
[27] A.K. Nayak, R.A. Shenoi, S.S.J. Moy, Transient response of composite sandwich plates, *Composite Structures* 64 (2004) 249–267.
[28] V.S. Rao, B.V. Sankar, C.T. Sun, Constrained layer damping of initially stressed composite beams using finite elements, *Journal of Composite Materials* 26 (1992) 1752–1766.
[29] T.P. Khatua, Y.K. Cheung, Stability analysis of multilayer sandwich structures, *AIAA Journal* 11 (1973) 1233–1234.
[30] O. Polit, M. Touratier, High-order triangular sandwich plate finite element for linear and non-linear analyses, *Computer Methods in Applied Mechanics and Engineering* 185 (2000) 305–324.
[31] S.M. Dickinson, The flexural vibration of rectangular orthotropic plates subjected to inplane forces, *Journal of Applied Mechanics* 36 (1969) 101–112.
[32] A.K. Noor, J.M. Peters, W.S. Burton, Three dimensional solutions for initially stressed structural sandwiches, *Journal of Engineering Mechanics* 120 (1994) 284–303.